Biochem. J. (2010) **430**, 265–274 (Printed in Great Britain) doi:10.1042/BJ20100181

online data

Substrate-specific binding and conformational changes involving Ser^{313} and transmembrane domain 8 of the human reduced folate carrier, as determined by site-directed mutagenesis and protein cross-linking

Zhanjun HOU*, Jianmei WU*, Jun YE†, Christina CHERIAN* and Larry H. MATHERLY*†‡§[1]

*Developmental Therapeutics Program, Barbara Ann Karmanos Cancer Institute, Wayne State University School of Medicine, Detroit, MI 48201, U.S.A., †Department of Biochemistry and Molecular Biology, Wayne State University School of Medicine, Detroit, MI 48201, U.S.A., ‡Graduate Program in Cancer Biology, Wayne State University School of Medicine, Detroit, MI 48201, U.S.A., and §Department of Pharmacology, Wayne State University School of Medicine, Detroit, MI 48201, U.S.A.

RFC (reduced folate carrier) is the major transporter for reduced folates and antifolates [e.g. MTX (methotrexate)]. RFC is characterized by two halves, each with six TMD (transmembrane domain) α helices connected by a hydrophilic loop, and cytoplasmic N- and C-termini. We previously identified TMDs 4, 5, 7, 8, 10 and 11 as forming the hydrophilic cavity for translocation of (anti)folates. The proximal end of TMD8 (positions 311–314) was implicated in substrate binding from scanning-cysteine accessibility methods; cysteine replacement of Ser^{313} resulted in loss of transport. In the present study, Ser^{313} was mutated to alanine, cysteine, phenylalanine and threonine. Mutant RFCs were expressed in RFC-null R5 HeLa cells. Replacement of Ser^{313} with cysteine or phenylalanine abolished MTX transport, whereas residual activity was preserved for the alanine and threonine mutants. In stable K562 transfectants, S313A and S313T RFCs showed substantially decreased V_{max} values without changes in K_t values for MTX compared with wild-type RFC. S313A and S313T RFCs differentially impacted binding of ten diverse (anti)folate substrates. Cross-linking between TMD8 and TMD5 was studied by expressing cysteine-less TMD1–6 (N_6) and TMD7–12 (C_6) half-molecules with cysteine insertions spanning these helices in R5 cells, followed by treatment with thiol-reactive homobifunctional cross-linkers. C_6–C_6 and N_6–N_6 cross-links were seen for all cysteine pairs. From the N_6 and C_6 cysteine pairs, Cys^{175}/Cys^{311} was cross-linked; cross-linking increased in the presence of transport substrates. The results of the present study indicate that the proximal end of TMD8 is juxtaposed to TMD5 and is conformationally active in the presence of transport substrates, and TMD8, including Ser^{313}, probably contributes to the RFC substrate-binding domain.

Key words: antifolate, cross-linking, folate, major facilitator superfamily, mutagenesis, oligomer, reduced folate carrier, transporter.

INTRODUCTION

Folates are members of the B class of vitamins that are co-factors for the synthesis of nucleotide precursors, serine and methionine in one-carbon transfer reactions [1]. Mammalian cells, unlike bacteria, cannot synthesize folates *de novo*. Hence, folate requirements must be met entirely from dietary sources [2,3]. Because of their hydrophilic charged character, there is minimal passive diffusion of anionic folates across cell membranes. Accordingly, specific transporters have evolved to mediate intestinal absorption of dietary folates, renal tubular secretion and reabsorption of folates, and transport of circulating reduced folates into systemic tissues [3].

The ubiquitously expressed RFC (reduced folate carrier) is considered to be the major transport system for folate co-factors in mammalian cells and tissues [3,4]. RFC serves a generalized role in folate transport and provides specialized tissue functions [5–9] such that loss of RFC expression or function may have potentially profound physiological and developmental consequences associated with folate deficiency [10]. RFC is also a major transporter of antifolate drugs used for cancer chemotherapy such as MTX (methotrexate), pemetrexed and raltitrexed [4]. Furthermore, the effectiveness of chemotherapy with these agents is closely linked to levels and activity of RFC in tumours [4,11].

Transport protein structural information is a prerequisite for understanding the mechanism of membrane transport. RFC is a mammalian prototype of the MFS (major facilitator superfamily) of transporters [4] that includes a large group of carriers that mediate uptake of diverse substrates including amino acids, neurotransmitters, sugars, vitamins, nucleosides and organic phosphate [12]. MFS proteins typically contain 400–600 amino acids and a structural motif composed of two halves, each with six transmembrane-spanning α-helices connected by a large hydrophilic loop, and cytoplasmic N- and C-termini. X-ray crystallographic structures of the bacterial MFS proteins, lactose/proton symporter (LacY) [13] and inorganic phosphate/glycerol-3-phosphate antiporter (GlpT) [14], were reported in 2003 at resolutions of 3.5 Å (1 Å = 0.1 nm) and 3.3 Å respectively. In both the LacY and GlpT structures, hydrophilic cavities form substrate-binding sites from helices-I, -II, -IV and -V of the N-terminal domain, and helices-VII, -VIII, -X and -XI of the C-terminal domain. Helices-III, -VI, -IX and -XII are embedded in the lipid bilayer and are not directly involved in substrate binding.

By contrast, for mammalian MFS transporters such as RFC, structural data are limited due to difficulties in isolating sufficient quantities of purified proteins and in crystallizing proteins for X-ray diffraction studies. With hRFC (human RFC), we used scanning cysteine mutagenesis to generate 282 mutants

Abbreviations used: BMH, 1,6-bis(maleimido)hexane; C_6, transmembrane domains 7–12; *cl*, cysteine-less; HA, haemagglutinin; MFS, major facilitator superfamily; MTSES, 2-sulfonatoethyl methanethiosulfonate; MTX, methotrexate; N_6, transmembrane domains 1–6; *p*-PDM, *p*-phenylenedimaleimide; RFC, reduced folate carrier; hRFC, human RFC; TMD, transmembrane domain; *wt*, wild-type.

[1] To whom correspondence should be addressed (email matherly@kci.wayne.edu).

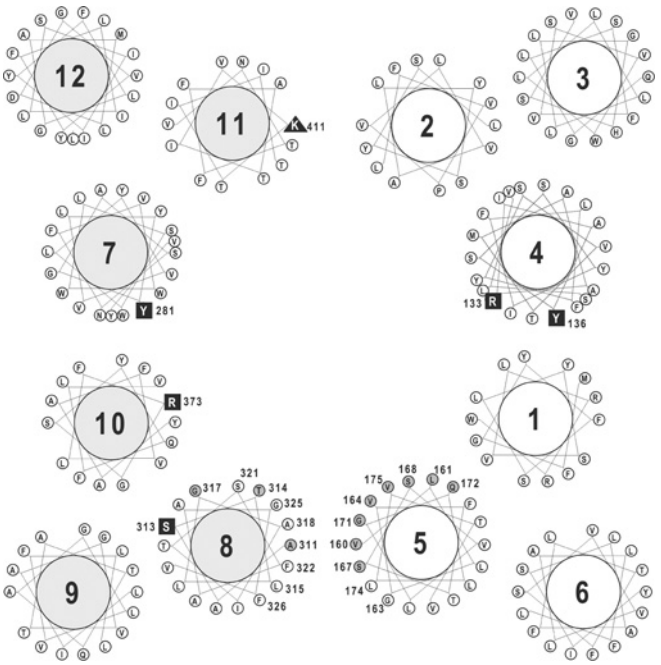

Figure 1 Two-dimensional structural model of hRFC

A two-dimensional model for hRFC is shown based on the solved crystal structures of LacY and GlpT and scanning-cysteine accessibility methods [16]. The 12 TMDs of hRFC are divided into two distinct segments, forming N- (TMD1–6) and C- (TMD7–12) terminal six-helix bundles. At the interface between the two segments, a hydrophilic cavity is formed from TMDs 1, 2, 4 and 5 of the N-terminal segment and TMDs 7, 8, 10 and 11 of the C-terminal segment. TMDs 3, 6, 9 and 12 face the lipid bilayer and are not exposed to this aqueous cavity. Residues of the TMD5 and TMD8 helices targeted in our study for cysteine-scanning mutagenesis and cross-linking are numbered. Numbered positions in grey circles designate aqueous-accessible residues shown by scanning cysteine accessibility methods in our previous publications [15,16]. Residues for which cysteine substitutions result in non-functional mutant hRFCs [15,16] are indicated as black squares. Lys^{411} in TMD11 is labelled as a black triangle, reflecting its unique role in transport substrate binding, as reported previously [33].

with cysteine residues individually inserted into TMDs (transmembrane domains) 1–12 [15,16]. For the active 272 mutants, aqueous accessibilities were confirmed by monitoring transport and protective effects of substrate [leucovorin or (6*R*,*S*)-5-formyl tetrahydrofolate] upon treatment with membrane-impermeable MTSES (2-sulfonatoethyl methanethiosulfonate). By homology modelling from the solved structures for bacterial MFS proteins and results of biochemical studies, a three-dimensional structural model for the hRFC monomer was generated that includes TMDs 1, 2, 4, 5, 7, 8, 10 and 11 as components of an aqueous membrane-spanning translocation pathway flanked by TMDs 3, 6, 9 and 12. A two-dimensional model of helix packing for monomeric hRFC that incorporates these features is presented in Figure 1. Most recently, hRFC monomers were found to form homo-oligomers [17].

While powerful, scanning-cysteine accessibility methods provide only modest detailed information on the roles of individual residues in substrate binding and/or membrane translocation, let alone dynamic structural changes in the carrier that accompany substrate binding. In our cysteine-scanning studies for hRFC, the ten inactivating cysteine substitutions included a stretch of residues in TMD4 (Arg^{133}, Ile^{134}, Ala^{135}, Tyr^{136} and Ser^{138}), Tyr^{281} in TMD7, Ser^{313} in TMD8 and Arg^{373} in TMD10, suggesting their functional or structural importance [16]. Of particular interest is Ser^{313}, flanking MTSES-reactive positions 311 and 314 in the proximal (extracellular) end of TMD8 which lines the aqueous transmembrane pathway for hRFC. In murine RFC, replacement of the homologous Ser^{309} with phenylalanine resulted in loss of MTX transport and MTX resistance, although the extent of the transport defect varied with different transport substrates [18].

In the present study, we use systematic site-directed mutagenesis for Ser^{313}, and cysteine-insertion mutagenesis and homobifunctional cross-linking between TMD8 and juxtaposed TMD5 to explore the functional significance of TMD8 and Ser^{313} in membrane transport by hRFC. Our results indicate substantial differences between various (anti)folate substrates in their binding to hRFCs with mutated Ser^{313}, and in inducing conformational changes involving the proximal end of TMD8 by protein cross-linking, in direct support of a essential role for this region and Ser^{313} in binding and/or membrane translocation of (anti)folate substrates.

MATERIALS AND METHODS

Reagents

[3′,5′,7-^{3}H]MTX (20 Ci/mmol) was purchased from Moravek Biochemicals. The sources of the classical antifolate drugs were as follows: MTX and aminopterin (Drug Development Branch, National Cancer Institute, Bethesda, MD, U.S.A.); edatrexate (10-ethyl-10-deazaaminopterin; CIBA-GEIGY Corporation); PT523 [N^{α}-(4-amino-4-deoxypteroyl)-N^{δ}-hemiphthaloyl-L-ornithine from Dr Andre Rosowsky (Dana Farber Cancer Institute, Boston, MA, U.S.A.)]; raltitrexed (*N*-{5-[*N*-(3,4-dihydro-2-methyl-4-oxyquinazolin-6-ylmethyl)-*N*-methyl-amino]-2-thienoyl}-L-glutamic acid) and ZD9331 [(2*S*)-2-{*O*-fluoro-*p*-[*N*-(2,7-dimethyl-4-oxo-3,4-dihydro-quinazolin-6-ylmethyl)-*N*-(prop-2-ynyl)amino]benzamido}-4-(tetrazol-5-yl)-butyric acid] were from AstraZeneca Pharmaceuticals; lometrexol [(6*R*)-5,10-dideaza-5,6,7,8-tetrahydrofolate] and pemetrexed [*N*-{4-[2-(2-amino-3,4-dihydro-4-oxo-7H-pyrrolo[2,3-*d*]pyrimidin-5-yl)-ethyl]benzoyl}-L-glutamic acid] (Alimta) were from Eli Lilly; and GW1843U89 {(*S*)-2-[5-({[1,2-dihydro-3-methyl-1-oxo-benzo(f)quinazolin-9-yl] methyl} amino)1-oxo-2-isoindolinyl] glutaric acid} was from GlaxoSmithKline. Leucovorin and folic acid were purchased from Sigma Chemical Company. Both labelled and unlabelled MTX were purified by HPLC prior to use [19]. Synthetic oligonucleotides were obtained from Invitrogen. Tissue culture reagents and supplies were purchased from assorted suppliers with the exception of fetal bovine and iron-supplemented calf sera, which were purchased from Hyclone Technologies. *p*-PDM (*p*-phenylenedimaleimide) was purchased from Sigma Chemical Company and BMH [1,6-bis(maleimido)hexane] was obtained from Pierce Chemical Company.

Construction of *cl*-N_6/C_6 hRFC half-molecules with paired cysteine residues and hRFC Ser^{313} mutants

The previously described HA (haemagglutinin)-tagged TMD1–6 (N_6) and Myc-tagged TMD7–12 (C_6) half-molecule constructs in pcDNA3.1 and pcDNA3 respectively [20], were used as templates to construct cysteine-less (*cl*) N_6/C_6 hRFC (*cl*-N_6/C_6) devoid of cysteine residues. *cl* N_6 (*cl*-N_6) was prepared by replacing three cysteine residues (at positions 30, 33 and 220) of N_6 hRFC with serine by site-directed mutagenesis using the QuikChange® kit (Stratagene). *cl* C_6 (*cl*-C_6) hRFC was constructed by a combination of restriction digestions and site-directed mutagenesis. First, the SfiI–NotI fragment of C_6 hRFC in pcDNA3 was replaced with the corresponding DNA fragment from full-length *cl*-hRFC [21], resulting in replacement of three cysteine residues (at

position 365, 396 and 458) with serine. The fourth cysteine (at postion 246) was changed to serine by site-directed mutagenesis. Using *cl*-N_6 hRFC as a template, an analogous approach was used to insert single cysteine residues into TMD5 (positions 160, 161, 163, 164, 167, 168, 171, 172, 174 and 175). Similarly, single cysteine residues were inserted into TMD8 (311, 314, 315, 317, 318, 321, 322, 325 and 326) of *cl*-C_6 hRFC. Ser^{313} mutants of hRFC were constructed by site-directed mutagenesis from HA-tagged full-length wild-type (*wt*) hRFC ($hRFC^{HA}$) [22] using the QuikChange® mutagenesis kit. Mutagenesis primers are shown in Supplementary Table S1 (at http://www.BiochemJ.org/bj/430/430/bj4300265add.htm). All mutations were confirmed by DNA sequencing at the Wayne State University DNA Sequencing Facility.

Cell culture and hRFC transfections

Transport-defective MTX-resistant HeLa cells, designated R5 [23], were a gift from Dr I. David Goldman (Albert Einstein College of Medicine, Bronx, NY, U.S.A.). R5 cells were maintained in RPMI 1640 medium, supplemented with 10 % fetal bovine serum, 2 mM L-glutamine, penicillin (100 units/ml), and streptomycin (100 μg/ml) in a humidified atmosphere at 37 °C in the presence of 5 % CO_2. Transient transfections of *wt* and mutant hRFC constructs (see below) were performed with Lipofectamine™ Plus reagent (Invitrogen), as described previously [15,16]. Cultures were split 24 h after transfection and assayed for transport and expression on Western blots after an additional 24 h.

The MTX transport-deficient K562 subline, designated K500E, was selected from *wt* K562 cells (American Type Culture Collection) and maintained in complete RPMI 1640 medium containing 10 % iron-supplemented calf serum, 2 mM L-glutamine, 100 units/ml penicillin and 100 μg/ml streptomycin, and 0.5 μM MTX [24]. *Wt* and mutant hRFC constructs (see below) were transfected into K500E cells by electroporation (155 V, 1000 μF capacitance). After 24 h, cells were treated with G418 (1 mg/ml) and stable clones were selected by cloning in soft agar in the presence of G418 [24]. Both *wt* and transfected K500E cultures were cultured in complete RPMI 1640 with 10 % supplemented calf serum and antibiotics in a humidified atmosphere at 37 °C in the presence of 5 % CO_2. For transfected cells, the medium was supplemented with G418 (1 mg/ml).

Membrane transport assays

Uptake of [^{3}H]MTX (0.5 μM) in transiently transfected R5 HeLa cells was measured over 2 min at 37 °C in 60 mm dishes in HSM buffer (Hepes/sucrose/Mg^{2+} 'anion-free' buffer; 20 mM Hepes and 235 mM sucrose, pH adjusted to 7.14 with MgO). Uptake of [^{3}H]MTX was quenched with ice-cold Dulbecco's PBS. Cells were washed with ice-cold PBS (3 times) and proteins were solubilized with 0.5 M NaOH. [^{3}H]MTX uptake into stably transfected K500E cells was measured over 180 s (*wt* and Ser^{313} mutants) in physiological HBSS (Hank's balanced salts solution) in a shaking water bath at 37 °C, as described previously [24,25]. For both cell line models, levels of intracellular radioactivity were expressed as pmol/mg of protein, calculated from direct measurements of [^{3}H]MTX and protein content of cell homogenates. Protein assays were based on the method of Lowry et al. [26]. For the stable transfected K500E cells, kinetic constants (K_t, V_{max}) were calculated from Lineweaver–Burk plots for [^{3}H]MTX, and K_i values for assorted transport substrates were determined from Dixon plots with [^{3}H]MTX (1 μM).

Preparation of plasma membranes and protein cross-linking

Transfected cells were harvested, flash-frozen and stored at − 80 °C. Plasma membranes were prepared from the frozen cell pellets as described previously [25]. Membrane preparations used for cross-linking were suspended in 20 mM Tris/HCl (pH 7.5) containing 100 mM sucrose with a protease inhibitor cocktail (Roche) at a protein concentration of 1–2 mg/ml. Otherwise, membrane preparations were suspended in the aforementioned buffer without sucrose. Membrane preparations were stored at − 80 °C as aliquots for further use.

Both *in vitro* (plasma membranes) and *in vivo* (transfected cells) cross-linking reactions were performed at 4 °C or 25 °C with thiol-specific homobifunctional cross-linkers [*p*-PDM (10 Å; rigid) or BMH (16 Å; flexible)]. Final concentrations of cross-linkers were 1 mM (*in vitro* cross-linking) or 0.25 mM (cross-linking with intact cells) and treatments were for 30 min. Reactions were terminated by adding 10 mM dithiothreitol. For the cell treatments, following cross-linking, membranes were prepared. In either case, membranes were diluted into SDS/PAGE sample buffer [62.5 mM Tris/HCl (pH 6.8), 10 % glycerol, 0.7 % SDS and 0.7 M 2-mercaptoethanol] and analysed by SDS/PAGE (10 % gels) [15]. Proteins were transferred on to PVDF membranes (Pierce) [15] and immunoblotted with Myc- or HA-specific monoclonal antibodies (Covance) against epitope-tagged C_6 and N_6 hRFC proteins respectively, and anti-mouse secondary IRDye™ 800-conjugated antibody (Rockland). Detection and densitometry used the Odyssey® IR imaging system and software (LI-COR Biosciences).

For studies of substrate-induced conformational changes, cells or membranes were incubated with transport substrates (1 mM final concentration) at room temperature (25 °C for 10 min and 1 h respectively), followed by cross-linking and immunoblotting, as described above.

In some experiments, proteins were digested with *N*-glycosidase F (New England Biolabs) prior to SDS/PAGE. For this, membranes were collected by ultracentrifugation (48 000 rev./min; TLA 100.2 rotor and Beckman TL100 ultracentrifuge) after cross-linker treatment and resuspended in 10 mM Tris/HCl (pH 7.5) containing the protease inhibitor cocktail. Samples were denatured for 10 min with 0.5 % SDS and 40 mM dithiothreitol. An equal volume of 50 mM sodium phosphate (pH 7.5) and 1 % Nonidet P40 were added, along with *N*-glycosidase F (1000 units), followed by incubation at 37 °C for 14 h. Control samples were incubated in parallel in buffer without *N*-glycosidase F. Samples were diluted with 3× SDS/PAGE sample buffer, fractionated on 10 % polyacrylamide gels, and analysed by Western blotting.

RESULTS AND DISCUSSION

Functional impact of conservative and non-conservative replacements of Ser^{313} in TMD8 of hRFC

Ser^{313} is located in the proximal end of TMD8. In murine RFC, replacement of Ser^{309} (homologous with Ser^{313} in hRFC) with phenylalanine resulted in loss of transport and MTX resistance, although the transport phenotype showed substantial substrate dependence [18]. Replacement of Ser^{313} in hRFC with cysteine was inactivating [16].

To further explore the potential role of Ser^{313} in binding and translocation of hRFC substrates, we performed systematic site-directed mutagenesis of this residue using HA-tagged *wt* hRFC as a PCR template. Both conservative and non-conservative replacements of Ser^{313} were tested, including alanine, cysteine and threonine, and results were compared with those for the

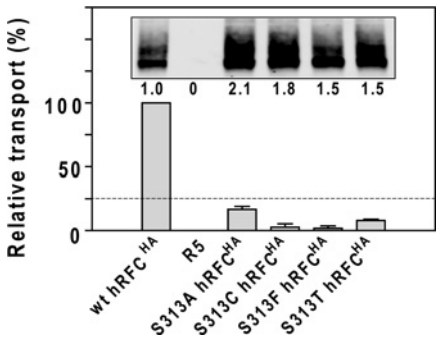

Figure 2 Expression and transport function of Ser[313] mutants

Transport activity and Western blotting results are shown for position 313 hRFC mutants transiently transfected into R5 HeLa cells. In the inset are shown results for a Western blot of hRFC proteins (2.5 μg of protein) solubilized from membrane preparations from R5 HeLa cells transiently transfected with *wt* and Ser[313] mutant hRFC constructs. Detection was with an HA-specific mouse antibody. Relative hRFC expression levels as determined by densitometry are shown below each lane. In the main panel are shown uptake data for [^{3}H]MTX (0.5 μM) over 2 min at 37 °C, normalized to hRFC protein levels from Western blots. Transport results are the means $\pm$ S.E.M. for three separate experiments.

Table 1 MTX kinetic parameters for *wt*, S313A and S313T hRFCs

Data are means $\pm$ S.E.M. for three separate experiments. For the normalized V_{max}, V_{max}/K_t parameters, calculated V_{max} values were normalized to relative hRFC levels on Western blots (Supplementary Figure S1 at http://www.BiochemJ.org/bj/430/bj4300265add.htm), measured by densitometry.

Transfectant	V_{max} (pmol/mg of protein per min)	Normalized V_{max}	K_t (μM)	V_{max} (normalized)/K_t
wt	4.62 $\pm$ 0.37	4.62 $\pm$ 0.37	1.89 $\pm$ 0.43	2.44
S313A	0.50 $\pm$ 0.04	0.41 $\pm$ 0.03	2.26 $\pm$ 0.44	0.18
S313T	0.81 $\pm$ 0.14	0.91 $\pm$ 0.16	2.11 $\pm$ 0.54	0.43

phenylalanine hRFC mutant, based on the published report on murine RFC [18]. All mutants were expressed in hRFC-null R5 HeLa cells at high levels on Western blots probed with an HA-specific antibody (Figure 2, inset). However, when assayed for transport with [^{3}H]MTX, all replacements were poorly tolerated. When transport results were normalized to levels of hRFC protein on Western blots, S313A and S313T preserved significant albeit low level activity over vector control-transfected cells with activities ~17 % and ~8 % respectively, of that for *wt* hRFC levels (Figure 2).

To characterize the role of Ser[313] in the specificity of substrate binding to hRFC, we generated stable transfectants of the S313A and S313T hRFC mutants in hRFC-null K562 (K500E) cells. The levels of hRFC proteins for vector control K500E, and for K500E cells transiently transfected with *wt*, S313A and S313T hRFCs were measured on Western blots and are shown in Supplementary Figure S1 (at http://www.BiochemJ.org/bj/430/bj4300265add.htm). Kinetic constants (K_t, V_{max} and V_{max}/K_t, including normalized values) for MTX with S313A and S313T hRFC, along with results for *wt* hRFC, were calculated from Lineweaver–Burke plots and are summarized in Table 1. The results show that K_t values for MTX were minimally changed from the *wt* values, whereas the V_{max} values were substantially decreased (Table 1).

To extend our kinetic analyses to additional transport substrates with disparate structures, we used ten (anti)folate substrates (raltitrexed, pemetrexed, leucovorin, folic acid, lometrexol, GW1843U89, PT523, ZD9331, aminopterin and edatrexate) as competitive inhibitors of [^{3}H]MTX (1 μM) uptake over a range of concentrations with *wt*, S313A and S313T hRFC-expressing cells. K_i values were calculated from Dixon plots (Table 2). Whereas K_i values for *wt* and mutant hRFCs were essentially identical for lometrexol, PT523, ZD9331 and edatrexate, statistically significant differences in binding were seen with other substrates. For instance, both S313A and S313T showed significantly decreased K_i values for pemetrexed, leucovorin and aminopterin (~2–3-fold) compared with those for *wt* hRFC. S313T hRFC showed selectively increased binding for raltitrexed and GW1843U89 compared with *wt* hRFC (~2–3-fold decreased K_i values), whereas S313A showed a ~2-fold increased K_i for folic acid compared with *wt* carrier. These results support the notion that Ser[313] located in the proximal end of TMD8 of hRFC directly participates in (anti)folate binding.

Table 2 K_i values for (anti)folate substrates

Data are means $\pm$ S.E.M. for three separate experiments. Statistically significant differences compared with K_i values for *wt* hRFC are noted as $^*P < 0.05$ and $^{**}P < 0.005$.

(Anti)folate	K_i (μM) *wt*	S313A	S313T
Raltitrexed	6.49 $\pm$ 0.35	7.01 $\pm$ 0.95	3.19 $\pm$ 0.26*
Pemetrexed	17.39 $\pm$ 1.10	8.80 $\pm$ 0.93*	4.58 $\pm$ 0.77*
Leucovorin	18.75 $\pm$ 1.54	12.30 $\pm$ 0.88*	7.74 $\pm$ 0.66*
Folic acid	193.68 $\pm$ 5.45	434.52 $\pm$ 82.69*	237.29 $\pm$ 58.38
Lometrexol	6.66 $\pm$ 0.67	7.21 $\pm$ 1.07	4.50 $\pm$ 0.60
GW1843U89	2.10 $\pm$ 0.01	2.61 $\pm$ 0.50	0.75 $\pm$ 0.06**
PT523	4.56 $\pm$ 0.97	3.13 $\pm$ 0.17	2.86 $\pm$ 0.85
ZD9331	4.42 $\pm$ 0.93	2.96 $\pm$ 0.52	2.31 $\pm$ 0.18
Aminopterin	7.03 $\pm$ 0.02	3.43 $\pm$ 0.58*	2.75 $\pm$ 0.15**
Edatrexate	5.48 $\pm$ 1.10	4.25 $\pm$ 0.53	2.23 $\pm$ 0.38

Characterization of functional *cl*-N_6/C_6 hRFC half-molecule transporter

TMDs 8 and 5 are juxtaposed in our hRFC monomer models (Figure 1). We previously reported that cysteine substitutions at multiple positions in TMD5 (Val[160], Leu[161], Val[164], Ser[167], Ser[168], Gly[171], Gln[172], Val[175]) and TMD8 (Ala[311], Thr[314]) were reactive with MTSES [16]. Although substrate protection from MTSES was variable among these positions, the protection afforded T314C was particularly notable (2.1-fold) [16]. These results unambiguously established aqueous accessibilities for positions spanning the entire length of TMD5 and in the proximal end of TMD8 in hRFC, and they strongly implied that Thr[314] in TMD8 faces the substrate-binding pocket (Figure 1).

Our immediate goal was to express functional *cl*-hRFC as TMD1–6 and TMD7–12 half-molecules (designated N_6 and C_6 respectively) in hRFC-null R5 cells, *cl*-N_6 with an HA insertion after Glu[226] and *cl*-C_6 with a Myc-His_{10} inserted after Leu[537] (Figure 3A). For cross-linking, *cl*-N_6 and *cl*-C_6 hRFC constructs were mutated to include cysteine insertions at defined positions spanning the lengths of helices 5 and 8. This approach was based on our previous report that co-expression of *wt* hRFC half molecules (*wt*-N_6/C_6) in hRFC-null cultured human cells led to functional complementation and restoration of transport activity, whereas transfections with the N_6 or C_6 hRFC constructs individually were ineffective [20]. The expressed HA-tagged hRFC N_6 fragment was glycosylated at Asn[58], resulting in a broadly banding (27–58 kDa) pattern on SDS/PAGE that quantitatively reverted to a 27 kDa species upon

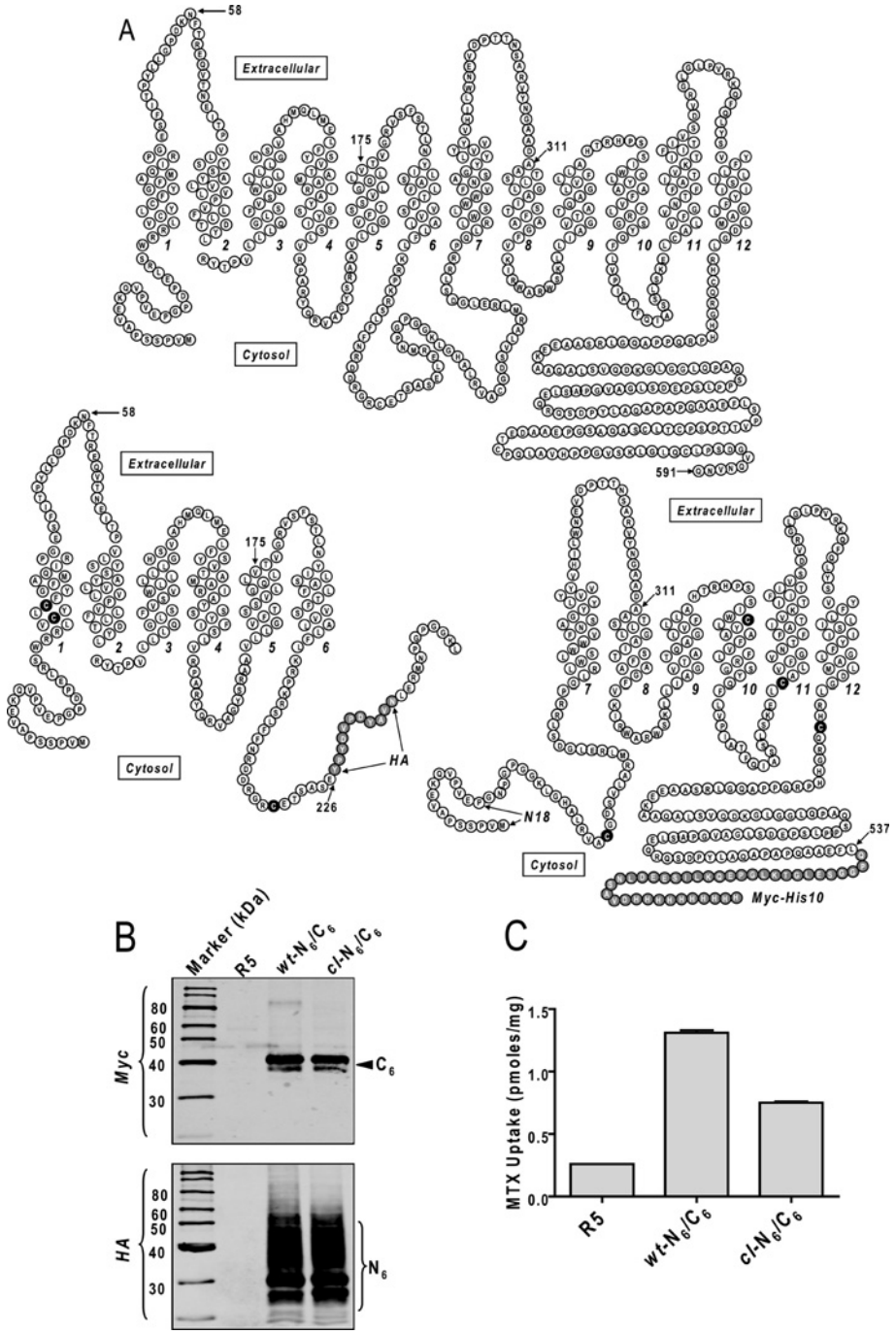

Figure 3 Schematic diagrams of full length *wt* hRFC and hRFC-TMD1–6 and hRFC-TMD7–12 half molecules; expression and transport of *cl*-N_6/C_6 in R5 cells

(**A**) The upper panel shows a topology model for full-length *wt* hRFC, based on the predicted hRFC amino acid sequence including 12 TMDs, internally oriented N- and C-terminal domains, and a cytosolic loop connecting TMDs 6 and 7. Amino acids are designated by the single letter abbreviations. The lower left-hand panel shows the structure of the hRFC TMD1–6 protein in which the 11 amino acid (YPYDVPDYAVN) HA epitope is inserted at position 226. The lower right-hand panel shows the structure of the hRFC TMD7–12 protein in which a Myc–His_{10} epitope is inserted at position 537. This construct was also designed to include 18 amino acids (MVPSSPAVEDKQVPVEP) from the N-terminus of hRFC (designated N18 in the figure). The seven cysteine residues in the hRFC half-molecule proteins are shown as black circles. (**B**) Western blot of membrane proteins (2.5 μg of protein) from R5 cells, and from R5 cells transfected with *wt*-N_6/C_6 and *cl*-N_6/C_6. Detection involved anti-Myc antibody (upper panel) or anti-HA antibody (lower panel), and IRDye800-conjugated secondary antibody. The molecular mass in kDa is indicated on the left-hand side of the gels. (**C**) Results for levels of [^{3}H]MTX (0.5 μM) uptake in R5 cells and in R5 transfectants expressing *cl*-N_6/C_6 and *wt*-N_6/C_6. Transport results are expressed as the means $\pm$ ranges for duplicate experiments.

enzymic deglycosylation, whereas the Myc-tagged hRFC C_6 half-molecule migrated as a sharp 40 kDa band on SDS/PAGE [20]. Confocal analysis showed that when co-expressed, both the N_6 and C_6 half-molecules were targeted to the plasma membrane with no obvious intracellular staining [20].

We initially needed to prepare the *cl*-N_6/C_6 hRFC construct, for which we used *wt*-N_6/C_6 hRFCs as a template for cysteine replacements. *cl* half-molecule constructs were generated by replacing cysteine residues at positions 30, 33 and 220 in N_6, and at positions 246, 365, 396 and 458 in C_6 with serine (Figure 3A).

cl-N_6/C_6 was co-transfected into hRFC-null R5 Hela cells to test for restoration of transport function and hRFC protein expression. *wt*-N_6/C_6 was transfected in parallel as a positive control. At 48 h post-transfection, cells were harvested for assays of [^{3}H]MTX transport and levels of individual *wt*- and *cl*- N_6 and C_6 proteins on Western blots with antibodies against HA and Myc epitopes respectively.

As shown in Figure 3(B) (lower panel), a major band migrating at 30 kDa was detected with an anti-HA antibody (detects N_6 hRFC) for both *wt*-N_6/C_6 and *cl*-N_6/C_6 hRFCs, along with an assortment of higher molecular mass N-glycosylated N_6 forms. With the anti-Myc antibody (detects C_6 hRFC; Figure 3B, upper panel), a major 40 kDa band was detected for both *wt*-N_6/C_6 and *cl*-N_6/C_6. An unidentified low abundant (~38 kDa) species was detected with anti-Myc antibody in some analyses. Although there were nominal differences in expression of N_6 and C_6 between *wt*- and *cl*-hRFC proteins, MTX transport was somewhat decreased (~40 %) for *cl*-N_6/C_6 (Figure 3C). Nonetheless, the MTX uptake for *cl*-N_6/C_6 still exceeded (~3-fold) the residual low level in R5 cells.

Preparation and cross-linking of N_6/C_6 hRFC with paired cysteine residues in TMD5/TMD8

The use of functional *cl*-N_6/C_6 with each half-molecule including a unique epitope tag and strategically placed cysteine insertions provided an ideal approach for identifying cross-linked domains, simply by following changes in migrations of HA- and Myc-tagged proteins on Western blots. Although there may be slight differences in folding between reconstituted half-molecule transporters and full-length *wt* hRFC, *wt*-N_6/C_6 hRFC was shown to accurately recapitulate a number of functional characteristics of full-length *wt* hRFC [20].

Based on their relative proximities and proposed orientations toward the hRFC hydrophilic cavity in two- (Figure 1) and three-dimensional [16] models, cysteine residues were inserted into *cl*-N_6/C_6 along the juxtaposed faces of TMD5 in N_6 hRFC (positions 175, 174, 172, 171, 168, 167, 164, 163, 161 and 160) and of TMD8 in C_6 hRFC (positions 311, 314, 315, 317, 318, 321, 322, 325 and 326) (Figure 4A). Altogether, ten cysteine N_6/C_6 pairs (175/311, 174/314, 172/315, 171/317, 168/318, 167/321, 164/322, 163/325, 161/326 and 160/326 in TMDs 5/8) were selected for transfections of hRFC-null R5 cells. All of the N_6/C_6 double cysteine mutants were expressed in R5 cells and the six cysteine mutant pairs (175/311, 174/314, 172/315, 168/318, 164/322 and 160/326) with transport activities in excess ($\geqslant$2-fold) of the basal low level in untransfected cells (Supplementary Figure S2 at http://www.BiochemJ.org/bj/430/bj4300265add.htm) were used for cross-linking experiments (Figure 4A also shows a schematic of the cysteine pairs used for cross-linking).

For the initial cross-linking experiments, plasma membranes were prepared and cross-linked *in vitro* at 25 °C with the membrane-permeable homobifunctional cross-linkers *p*-PDM and BMH [27]. The proteins were separated by SDS/PAGE for Western analysis with a Myc-specific antibody. In the absence of cross-linkers, a prominent ~40 kDa species was detected (Figure 5A, lane 4 shows this result for the Cys^{175}/Cys^{311} pair). For the Cys^{175} N_6 and Cys^{311} C_6 mutant pair, treatment with cross-linkers resulted in two major bands [70 and 80 kDa; labelled N_6–C_6 and C_6–C_6 respectively, in Figures 4B (lanes 1 and 2) and 5A (lanes 5 and 6)] not seen in the absence of cross-linkers (Figure 5A, lane 4) or in *cl*-N_6/C_6 in the presence or absence of cross-linkers (Figure 5A, lanes 1–3). With the other five mutants, identical results were obtained in the absence of cross-linkers (results not shown). Although a very low level of the 70 kDa N_6–C_6 was

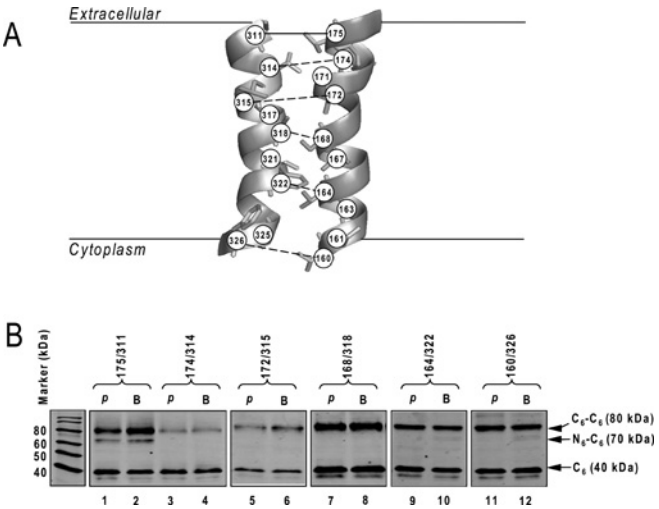

Figure 4 Chemical cross-linking of double-cysteine mutants of TMDs 5/8

(**A**) Functional cysteine pairs for cross-linking are shown on TMD helices 5/8 from a three-dimensional model of hRFC [16]. Paired cysteine residues that are cross-linked by *p*-PDM or BMH are connected with a solid line. Cysteine pairs which exhibit no cross-linking are connected with a broken line. (**B**) Western blots of cross-linked membrane samples of cysteine pairs from TMD helices 5/8 treated with *p*-PDM and BMH. Cross-linking reactions were performed with plasma membrane preparations *in situ* at 25 °C. The immunoblots were probed with anti-Myc antibody and IRDye800-conjugated secondary antibody, and were detected as described in the Materials and methods section. C_6 and cross-linked products (C_6–C_6 and N_6–C_6) are indicated by arrows. *p*, *p*-PDM; B, BMH. The molecular mass in kDa is indicated on the left-hand side of the gel.

detected with BMH and Cys^{160}/Cys^{326} with the anti-Myc antibody, for the other mutant pairs and cross-linkers, only the 80 kDa (C_6–C_6) species was detected (Figure 4B). Explanations for the failure to detect the 70 kDa band with these cysteine pairs range from their relative inaccessibilities to the cross-linkers or helix proximities somewhat different from those predicted by the three-dimensional hRFC model [16], to the impact of nearby amino acids on individual cysteine chemical reactivities, all of which may preclude an ability to efficiently cross-link, even though individual cysteine residues may be highly reactive. From their sizes, the 70 kDa and 80 kDa bands probably arose from cross-links between the N_6 and C_6 half-molecules and between two C_6 half-molecules respectively. There was no obvious difference in the extent of cross-linking between *p*-PDM and BMH.

For the Cys^{175}/Cys^{311} pair without cross-linker, HA-specific antibody identified products derived from N_6, including a major ~30 kDa form and higher mass N-glycosylated forms (Figure 5A, lower panel, lane 4). An identical pattern was seen with *cl*-N_6/C_6 with or without cross-linkers (Figure 5A, lower panel, lanes 1–3). With *p*-PDM/BMH treatments of Cys^{175}/Cys^{311}, the 70 kDa (but not 80 kDa) band was detected, along with a 60 kDa species and higher molecular mass (glycosylated) forms not seen in the absence of cross-linkers (Figure 5A, lower panel, lanes 5 and 6). *N*-glycosidase F treatment shifted the major HA immunoreactive bands from 70, 60 and 30 kDa to 67, 54 and 27 kDa respectively (Figure 5B, lanes 3 and 4), further establishing their N-glycosylation and probable identities as N_6–C_6, N_6–N_6 and N_6 respectively. *N*-glycosidase F treatment also shifted the 70 kDa N_6–C_6 band detected with anti-Myc antibody to 67 kDa but not the 80 kDa C_6–C_6 or the 40 kDa C_6 bands (results not shown). When probed with anti-HA antibody, the five other cysteine pairs (174/314, 172/315, 168/318, 164/322 and 160/326) gave results identical with those for Cys^{175}/Cys^{311} in the

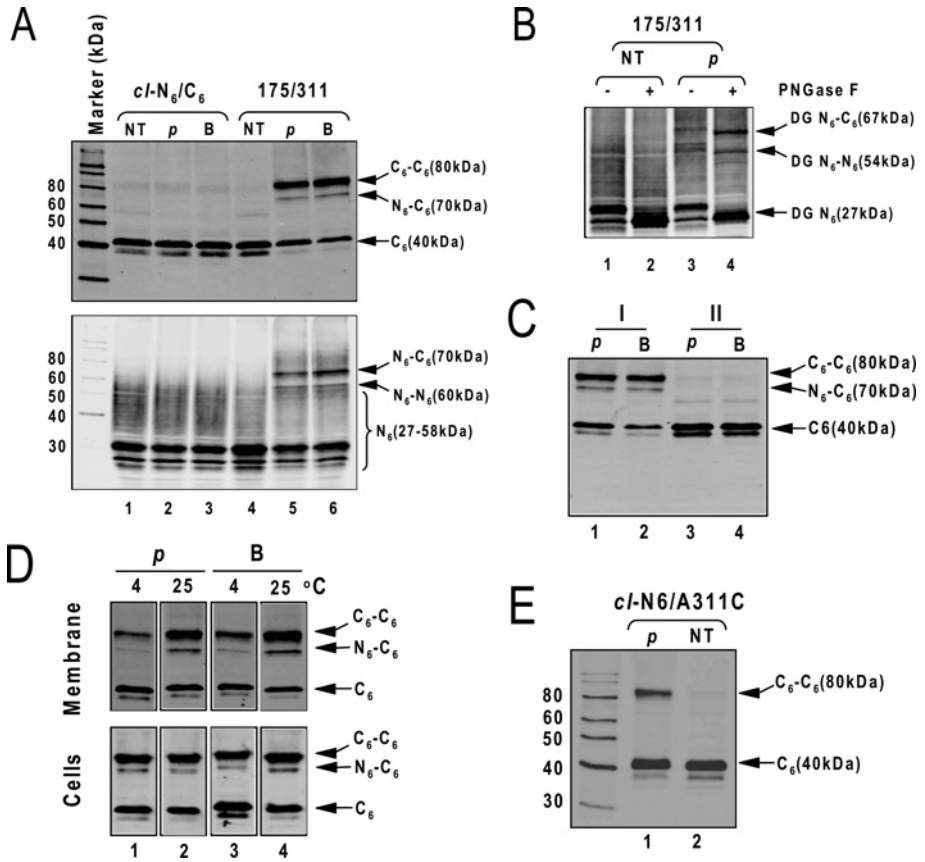

Figure 5 Validation of cross-linking with thiol-reactive homobifunctional cross-linkers

Chemical cross-linking of *cl*-N_6/C_6 and *cl*-N_6/C_6 including paired cysteine residues 175/311 from TMDs 5/8 was performed under a variety of conditions with *p*-PDM and BMH. Cross-linking was performed as described in the Materials and methods section. Membrane proteins were solubilized and analysed on Western blots. (**A**) Upper panel: cross-linking of *cl*-N_6/C_6 and *cl*-N_6/C_6 half-molecules containing paired Cys^{175}/Cys^{311} was performed on isolated plasma membranes under established conditions at 25 °C. The blot was probed with anti-Myc antibody. The C_6 fragment migrates at 40 kDa and the cross-linked N_6–C_6 and C_6–C_6 species migrate at 70 and 80 kDa respectively. Lower panel: the blot in the upper panel was stripped and re-probed with an anti-HA antibody. The major band corresponding to the N_6 fragment migrates as 30 kDa and the cross-linked N_6–N_6 and N_6–C_6 species migrate at approx. 60 and 70 kDa respectively. The molecular mass in kDa is indicated on the left-hand side. (**B**) Deglycosylation of cross-linked proteins with *N*-glycosidase F. Plasma membranes from R5 cells transfected with the Cys^{175}/Cys^{311} half-molecule constructs were either untreated or cross-linked with *p*-PDM at 25 °C, followed by digestion with or without *N*-glycosidase F. The immunoblot was probed with an HA-specific antibody and IRDye800-conjugated secondary antibody. (**C**) Controls for the cross-linking reaction are shown including: I, cross-linking at 25 °C of plasma membranes containing cysteine pair 175/311 under established conditions (lanes 1 and 2); and II, Cys^{175}/Cys^{311} plasma membranes solubilized with 0.7 % SDS before cross-linker treatment at 25 °C, followed by treatment with cross-linkers for 30 min and quenching with 10 mM dithiothreitol and SDS/PAGE buffer (lanes 3 and 4). The immunoblot was probed with an anti-Myc antibody. (**D**) Results are shown for cross-linking at 4 °C and 25 °C with isolated plasma membranes from transfected R5 cells expressing paired Cys^{175}/Cys^{311} half-molecules (upper panel) or intact transfected cells (lower panel) under established conditions at 4 °C and 25 °C. The immunoblot was probed with an anti-Myc antibody. (**E**) Results are shown for cross-linking at 4 °C with intact transfected R5 cells expressing *cl*-N_6 and Cys^{311} C_6 half-molecules. The immunoblot was probed with an anti-Myc antibody. *p*, *p*-PDM; *B*, BMH; NT, no treatment; PNGase, *N*-glycosidase F.

absence of cross-linking. Upon cross-linking, the 60 kDa species was detected (results not shown). Our inability to detect higher molecular mass (>70 kDa) glycosylated forms of N_6–C_6 on blots probed with anti-Myc antibody probably reflects differences in sensitivities between anti-Myc antibody and anti-HA antibody (as suggested from the more intense signal for the 70 kDa species with anti-HA over anti-Myc antibodies in Figure 5A).

Several critical controls were performed for our *in vitro* cross-linking experiments. When the reactions for Cys^{175}/Cys^{311} mutants were performed at 4 °C rather than 25 °C, cross-links were still detected (Figure 5D, upper panel, lanes 1 and 3). Another negative control involved solubilization of the Cys^{175}/Cys^{311} membranes with 0.7 % SDS before cross-linker treatment, followed by treatment with cross-linkers for 30 min at 25 °C, and quenching with 10 mM dithiothreitol and SDS/PAGE buffer (labelled II in Figure 5C, lanes 3 and 4). Results were compared with those for the Cys^{175}/Cys^{311} sample cross-linked under established conditions at 25 °C (labelled I in Figure 5C, lanes 1 and 2). For reaction II, neither the 70 kDa nor 80 kDa cross-linked band was detected (with anti-Myc antibody), firmly establishing that the cross-linking detected with the Cys^{175}/Cys^{311} half-molecules does not occur randomly in solution but rather can only occur *in situ* in the intact plasma membranes.

Cross-linking of the 175/311 cysteine pairs was also confirmed with intact cells co-transfected with Cys^{175} N_6 and Cys^{311} C_6 half-molecule constructs treated with *p*-PDM and BMH at 4 °C and 25 °C. In membrane preparations from cross-linked cells, both C_6–C_6 and N_6–C_6 cross-linked species were detected on Western blots (Figure 5D, lower panel). In cells co-transfected with the *cl*-N_6 and Cys^{311} C_6 half-molecule constructs and treated with *p*-PDM at 4 °C, the 80 kDa band (but not the 70 kDa band) was detected (Figure 5E, lane 1). This unambiguously establishes that the 80 kDa species (but not the 70 kDa form) is the result of cross-links between Cys^{311} on separate C_6 molecules and that the 70 kDa cross-linked product is absolutely dependent on co-expression of the Cys^{175} N_6 and Cys^{311} C_6 hRFC half-molecules.

Our cross-linking results strongly suggest that the TMD5 and TMD8 helices are close together at their proximal (extracellular) ends, as indicated by formation of the N_6–C_6 cross-link between Cys^{175} and Cys^{311}. Detection of C_6–C_6 intermolecular cross-links for multiple cysteine pairs spanning TMDs 5 and 8 suggests that the TMD8 helix in each hRFC half-molecule protomer abuts the corresponding region in another, in support of the notion of higher-order hRFC homo-oligomers, as recently reported [17]. An analogous argument can be made for the apparent N_6–N_6 intermolecular cross-links for the Cys^{175}/Cys^{311} pair and TMD5. While the formation of C_6–C_6 (or N_6–N_6) cross-links was completely unexpected given that the positions selected for cysteine replacement were based on their patterns of MTSES reactivities and apparent aqueous accessibilities, the nature of the homo-oligomeric interface(s) is not yet established. Studies are underway to explore this important question.

Effects of ligand binding on TMD5/TMD8 cross-linking as a sensitive probe of conformationally active interfaces

If Ser^{313} directly participates in substrate binding as suggested by our mutant studies, nearby residues (e.g. position 311) might be expected to be conformationally active in the presence of excess substrate. To test this possibility, *in situ* cross-linking involving position 311 was used as a highly sensitive probe of the conformationally active interfaces between transmembrane helices 8 and 5 upon substrate binding [28–30]. We transfected R5 cells with Cys^{175} N_6 and Cys^{311} C_6 hRFC, then treated the cells with BMH in the absence and presence of hRFC substrates (aminopterin, leucovorin and raltitrexed). In four independent experiments, N_6–C_6 (but not C_6–C_6) cross-links by BMH were demonstrably increased to 1.6-, 2.3- and 2.4-fold by leucovorin, aminopterin and raltitrexed respectively (Figure 6). Analogous results were observed with BMH-treated plasma membranes from Cys^{175}/Cys^{311}-transfected cells, cross-linked in the presence of transport substrates (Supplementary Figure S3 at http://www.BiochemJ.org/bj/430/bj4300265add.htm).

Since cross-link formation is a reflection of dynamic collisions that result in chemical modifications of reactive residues [31], our finding of enhanced cross-linking between positions 175 and 311 in the presence of transport substrates suggests that conformational changes occur involving the proximal end of TMD8 in relation to TMD5 upon substrate binding. This is entirely consistent with the notion that this stretch of TMD8 contributes to the substrate-binding pocket in hRFC, as noted above.

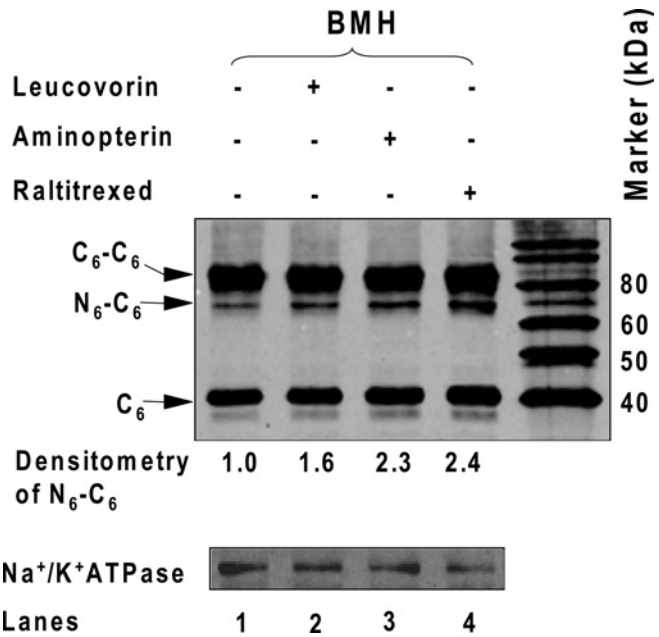

Figure 6 Effects of ligand binding on TMD5/TMD8 cross-linking

Intact R5 HeLa cells were transfected with paired Cys^{175}/Cys^{311} hRFC half-molecules, pre-treated with or without 1 mM aminopterin, leucovorin or raltitrexed at 25 °C for 10 min, followed by chemical cross-linking with BMH. The immunoblots were probed with an anti-Myc antibody and IRDye800-conjugated secondary antibody. Detection and densitometry were performed as described in the Materials and methods section. C_6 and cross-linked products (C_6–C_6 and N_6–C_6) are noted with arrows. In the lower panel, the blot was stripped and reprobed with an antibody against Na^+/K^+-ATPase as a loading control (mouse antibody from Novus Biologicals). Mean densitometry measurements of the intensities of the N_6–C_6 cross-linked band (normalized to respective loading controls) from four independent experiments are shown below each lane. Relative S.E.M. values were 0.10, 0.10 and 0.25 respectively for the leucovorin, aminopterin and raltitrexed treatments and *P* values compared with the no treatment were all less than 0.01, as measured using a paired *t* test. The molecular mass in kDa is indicated on the right-hand side of the gel.

Conclusions

Although hRFC exists as an homo-oligomer [17], each hRFC monomer has its own translocation pathway and appears to function independently [32]. Characterization of the determinants of substrate binding in each hRFC monomer is essential to understanding the molecular mechanism of folate and antifolate membrane transport by this physiologically and pharmacologically important carrier. We previously proposed that Lys^{411} in TMD11, Arg^{373} in TMD10, Tyr^{281} in TMD7 and Ser^{313} in TMD8 participate in (anti)folate binding and that TMD helices including these residues comprise the hRFC substrate-binding pocket [16]. Thus replacement of Arg^{373}, Tyr^{281} or Ser^{313} in hRFC individually with cysteine resulted in nearly complete loss of transport activity [16]. Similarly, aliphatic substitutions of Arg^{373} abolished transport, whereas activity was preserved with lysine replacement at this position [33]. Although Lys^{411} in hRFC can be replaced by any of a number of amino acids of varying bulk and charge with modest effects on transport activity, this residue is nonetheless the primary target for electrophilic attack by *N*-hydroxysuccinimide-activated MTX ester and can participate in an interaction with (anti)folate substrate, primarily through an ionic association with the γ-carboxy group [33]. However, this interaction with Lys^{411} is apparently not essential for transport function since the γ-carboxy group is not only expendable, but indeed its replacement by an uncharged hydrogen or methyl group in a series of furo[2,3-*d*]pyrimidine antifolates actually enhanced high-affinity reversible binding of substrate to the carrier, as long as an ionizable α-carboxy group is intact [33]. Rather, Arg^{373} was suggested to forge an ionic association with the α-carboxylate of (anti)folate substrates [33].

The present study sheds new important light on the functional significance of the proximal TMD8 helix in general, and Ser^{313} in particular. By kinetic analysis with an assortment of structurally diverse transport substrates, there were substrate-selective differences in K_i values between *wt* and Ala/Thr^{313} mutant hRFCs, suggesting a possible role for Ser^{313} in substrate binding to hRFC.

Our results with Cys^{175}/Cys^{311} hRFC half-molecule mutants and cysteine cross-linking established that the proximal (extracellular) ends of the TMD8 and 5 helices are juxtaposed, as predicted by hRFC homology models. Although cross-linking results must be interpreted with caution since cross-link formation is a reflection of dynamic movements and chemical reactivities with individual

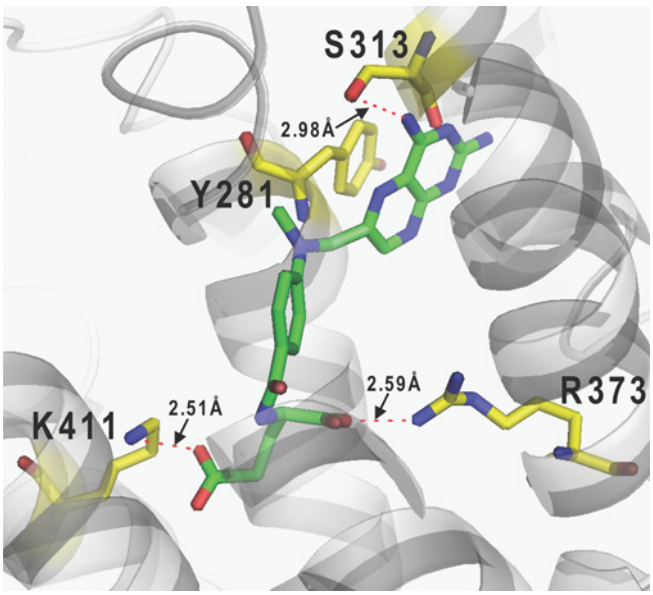

Figure 7 Hypothetical model of the hRFC binding pocket

A hypothetical model is shown for MTX binding to the proposed hRFC binding pocket. In this model, a MTX molecule (represented as green and blue sticks) was manually inserted into the hRFC substrate-binding pocket including Tyr^{281}, Ser^{313}, Arg^{373} and Lys^{411}, using the three-dimensional hRFC model described in our previous report [16]. Depicted are proposed interactions between the pteridine ring of MTX and Tyr^{281} and Ser^{313}, between the α-carboxy and Arg^{373}, and between the γ-carboxy and Lys^{411}. The estimated distances between the MTX molecule and the Ser^{313}, Arg^{373} and Lys^{411} side chains are noted.

cysteine residues rather than just their proximities [31], this approach has nonetheless established a close correlation between collision rates and residue proximities [34]. In the presence of transport substrates, the 175/311 interface was conformationally active, as reflected in increased N_6–C_6 cross-links between these positions. Thus while position 311 is not directly involved in substrate binding [16], this result nonetheless supports the notion that residues located in this stretch of TMD8 (i.e. Ser^{313}) participate in substrate binding. Cross-linking between Cys^{175} and Cys^{311} was substrate-dependent, further implying that hRFC assumes distinct conformations in this region upon binding different transport substrates, consistent with our kinetic analysis of structurally diverse transport substrates.

Based on these collective data, we present a hypothetical model for binding (anti)folate substrates to hRFC involving interactions between the pteridine ring of MTX and Tyr^{281} and Ser^{313}, and between the α-carboxy of MTX and Arg^{373} (Figure 7). Although a putative hydrogen bond is depicted between the Ser^{313} hydroxy group and the 4-amino group of MTX, this must not be obligatory since functionality at position 313 can in part met by alanine. In the model, Tyr^{281} is juxtaposed to the pteridine ring of MTX and may bind with MTX through π–π interactions. Lys^{411} interacts with the γ-carboxy group of MTX, although this is not essential for binding and transport, as noted above.

Finally, results are presented herein that C_6–C_6 and N_6–N_6 cross-links occur for the TMD5/8 cysteine pairs, providing further independent confirmation of the existence of homo-oligomeric hRFC [17]. As previously suggested, such higher-order hRFC structures should be particularly significant, with profound implications to hRFC mechanism, regulation and antifolate resistance [17]. Further characterization of the structural and regulatory features of homo-oligomeric hRFC will be the topic of future reports.

AUTHOR CONTRIBUTION

Zhanjun Hou designed and performed the experiments, and wrote the manuscript. Jianmei Wu prepared the Ser^{313} hRFC mutants, performed stable transfections of K500E cells and did the kinetic analysis. Jun Ye assisted with experimental design and generated the hypothetical molecular model of the hRFC substrate-binding site. Christina Cherian prepared the cysteine-less N_6 and C_6 half-molecule constructs and their cysteine insertion counterparts. Larry Matherly supervised the project and wrote the manuscript.

ACKNOWLEDGEMENTS

We would like to thank Dr I. David Goldman (Albert Einstein School of Medicine, Bronx, NY, U.S.A.) for his gift of hRFC-null R5 HeLa cells.

FUNDING

This work was supported by the National Cancer Institute, National Institutes of Health [grant number CA53535].

REFERENCES

1 Stokstad, E. L. R. (1990) In Folic Acid Metabolism in Health and Disease (Picciano, M. F., Stokstad, E. L. R. and Greogory, J. F., eds), pp. 1–21, Wiley-Liss, New York
2 Sirotnak, F. M. and Tolner, B. (1999) Carrier-mediated membrane transport of folates in mammalian cells. Annu. Rev. Nutr. **19**, 91–122
3 Matherly, L. H. and Goldman, D. I. (2003) Membrane transport of folates. Vitam. Horm. **66**, 403–456
4 Matherly, L. H., Hou, Z. and Deng, Y. (2007) Human reduced folate carrier: translation of basic biology to cancer etiology and therapy. Cancer Metastasis Rev. **26**, 111–128
5 Chiao, J. H., Roy, K., Tolner, B., Yang, C. H. and Sirotnak, F. M. (1997) RFC-1 gene expression regulates folate absorption in mouse small intestine. J. Biol. Chem. **272**, 11165–11170
6 Said, H. M. (2004) Recent advances in carrier-mediated intestinal absorption of water-soluble vitamins. Annu. Rev. Physiol. **66**, 419–446
7 Kneuer, C., Honscha, K. U. and Honscha, W. (2005) Rat reduced-folate carrier-1 is localized basolaterally in MDCK kidney epithelial cells and contributes to the secretory transport of methotrexate and fluoresceinated methotrexate. Cell Tissue Res. **320**, 517–524
8 Sweiry, J. H. and Yudilevich, D. L. (1985) Transport of folates at maternal and fetal sides of the placenta: lack of inhibition by methotrexate. Biochim. Biophys. Acta **821**, 497–501
9 Spector, R. and Johanson, C. (2006) Micronutrient and urate transport in choroid plexus and kidney: implications for drug therapy. Pharm. Res. **23**, 2515–2524
10 Matherly, L. H. (2004) Human reduced folate carrier gene and transcript variants: functional, physiologic, and pharmacologic consequences. Curr. Pharmacogenet. **2**, 287–298
11 Zhao, R. and Goldman, I. D. (2003) Resistance to antifolates. Oncogene **22**, 7431–7457
12 Saier, Jr, M. H., Beatty, J. T., Goffeau, A., Harley, K. T., Heijne, W. H., Huang, S. C., Jack, D. L., Jahn, P. S., Lew, K., Liu, J. et al. (1999) The major facilitator superfamily. J. Mol. Microbiol. Biotechnol. **1**, 257–279
13 Abramson, J., Smirnova, I., Kasho, V., Verner, G., Kaback, H. R. and Iwata, S. (2003) Structure and mechanism of the lactose permease of *Escherichia coli*. Science **301**, 610–615
14 Huang, Y., Lemieux, M. J., Song, J., Auer, M. and Wang, D. N. (2003) Structure and mechanism of the glycerol-3-phosphate transporter from *Escherichia coli*. Science **301**, 616–620
15 Hou, Z., Stapels, S. E., Haska, C. L. and Matherly, L. H. (2005) Localization of a substrate binding domain of the human reduced folate carrier to transmembrane domain 11 by radioaffinity labeling and cysteine-substituted accessibility methods. J. Biol. Chem. **280**, 36206–36213
16 Hou, Z., Ye, J., Haska, C. L. and Matherly, L. H. (2006) Transmembrane domains 4, 5, 7, 8, and 10 of the human reduced folate carrier are important structural or functional components of the transmembrane channel for folate substrates. J. Biol. Chem. **281**, 33588–33596
17 Hou, Z. and Matherly, L. H. (2009) Oligomeric structure of the human reduced folate carrier: identification of homo-oligomers and dominant-negative effects on carrier expression and function. J. Biol. Chem. **284**, 3285–3293
18 Zhao, R., Gao, F. and Goldman, I. D. (1999) Discrimination among reduced folates and methotrexate as transport substrates by a phenylalanine substitution for serine within the predicted eighth transmembrane domain of the reduced folate carrier. Biochem. Pharmacol. **58**, 1615–1624

19 Fry, D. W., Yalowich, J. C. and Goldman, I. D. (1982) Rapid formation of poly-γ-glutamyl derivatives of methotrexate and their association with dihydrofolate reductase as assessed by high pressure liquid chromatography in the Ehrlich ascites tumor cell *in vitro*. J. Biol. Chem. **257**, 1890–1896
20 Witt, T. L., Stapels, S. E. and Matherly, L. H. (2004) Restoration of transport activity by co-expression of human reduced folate carrier half-molecules in transport-impaired K562 cells: localization of a substrate binding domain to transmembrane domains 7–12. J. Biol. Chem. **279**, 46755–46763
21 Cao, W. and Matherly, L. H. (2003) Characterization of a cysteine-less human reduced folate carrier: localization of a substrate-binding domain by cysteine-scanning mutagenesis and cysteine accessibility methods. Biochem. J. **374**, 27–36
22 Payton, S. G., Haska, C. L., Flatley, R. M., Ge, Y. and Matherly, L. H. (2007) Effects of 5′ untranslated region diversity on the posttranscriptional regulation of the human reduced folate carrier. Biochim. Biophys. Acta **1769**, 131–138
23 Zhao, R., Chattopadhyay, S., Hanscom, M. and Goldman, I. D. (2004) Antifolate resistance in a HeLa cell line associated with impaired transport independent of the reduced folate carrier. Clin. Cancer Res. **10**, 8735–8742
24 Wong, S. C., McQuade, R., Proefke, S. A., Bhushan, A. and Matherly, L. H. (1997) Human K562 transfectants expressing high levels of reduced folate carrier but exhibiting low transport activity. Biochem. Pharmacol. **53**, 199–206
25 Matherly, L. H., Czajkowski, C. A. and Angeles, S. M. (1991) Identification of a highly glycosylated methotrexate membrane carrier in K562 human erythroleukemia cells up-regulated for tetrahydrofolate cofactor and methotrexate transport. Cancer Res. **51**, 3420–3426
26 Lowry, O. H., Rosebrough, N. J., Farr, A. L. and Randall, R. J. (1951) Protein measurement with the Folin phenol reagent. J. Biol. Chem. **193**, 265–275
27 Alisio, A. and Mueckler, M. (2004) Relative proximity and orientation of helices 4 and 8 of the GLUT1 glucose transporter. J. Biol. Chem. **279**, 26540–26545
28 Wu, J. and Kaback, H. R. (1997) Helix proximity and ligand-induced conformational changes in the lactose permease of Escherichia coli determined by site-directed chemical crosslinking. J. Mol. Biol. **270**, 285–293
29 Wu, J., Hardy, D. and Kaback, H. R. (1998) Tilting of helix I and ligand-induced changes in the lactose permease determined by site-directed chemical cross-linking *in situ*. Biochemistry **37**, 15785–15790
30 Wu, J., Hardy, D. and Kaback, H. R. (1998) Transmembrane helix tilting and ligand-induced conformational changes in the lactose permease determined by site-directed chemical crosslinking *in situ*. J. Mol. Biol. **282**, 959–967
31 Zhang, W., Guan, L. and Kaback, H. R. (2002) Helices VII and X in the lactose permease of *Escherichia coli*: proximity and ligand-induced distance changes. J. Mol. Biol. **315**, 53–62
32 Hou, Z., Cherian, C., Drews, J., Wu, J. and Matherly, L. H. (2009) Identification of the minimal functional unit of the homo-oligomeric human reduced folate carrier. J. Biol. Chem. **285**, 4732–4740
33 Deng, Y., Hou, Z., Wang, L., Cherian, C., Wu, J., Gangjee, A. and Matherly, L. H. (2008) Role of lysine 411 in substrate carboxyl group binding to the human reduced folate carrier, as determined by site-directed mutagenesis and affinity inhibition. Mol. Pharmacol. **73**, 1274–1281
34 Chervitz, S. A. and Falke, J. J. (1996) Molecular mechanism of transmembrane signaling by the aspartate receptor: a model. Proc. Natl. Acad. Sci. U.S.A. **93**, 2545–2550

Received 1 February 2010/8 June 2010; accepted 17 June 2010
Published as BJ Immediate Publication 17 June 2010, doi:10.1042/BJ20100181

Biochem. J. (2010) **430**, 265–274 (Printed in Great Britain) doi:10.1042/BJ20100181

online data

SUPPLEMENTARY ONLINE DATA

Substrate-specific binding and conformational changes involving Ser^{313} and transmembrane domain 8 of the human reduced folate carrier, as determined by site-directed mutagenesis and protein cross-linking

Zhanjun HOU*, Jianmei WU*, Jun YE†, Christina CHERIAN* and Larry H. MATHERLY*†‡§[1]

*Developmental Therapeutics Program, Barbara Ann Karmanos Cancer Institute, Wayne State University School of Medicine, Detroit, MI 48201, U.S.A., †Department of Biochemistry and Molecular Biology, Wayne State University School of Medicine, Detroit, MI 48201, U.S.A., ‡Graduate Program in Cancer Biology, Wayne State University School of Medicine, Detroit, MI 48201, U.S.A., and §Department of Pharmacology, Wayne State University School of Medicine, Detroit, MI 48201, U.S.A.

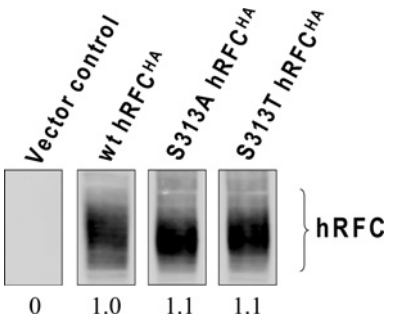

Figure S1 Expression of *wt*, S313A and S313T hRFC in K500E (K562) stable clones

Results are shown for a Western blot of plasma membrane proteins (10 μg of protein) from hRFC-null K500E cells stably transfected with *wt* hRFC, S313A hRFC and S313T hRFC. hRFC proteins were detected with an HA-specific mouse antibody and secondary IRDye^{TM} 800-conjugated antibody. Detection and densitometry of the blots was performed with the Odyssey® Imaging System. The relative hRFC expression level as determined by densitometry is shown below each lane.

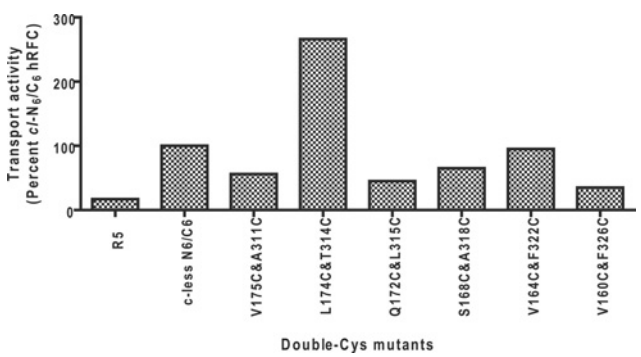

Figure S2 Transport activity for *cl*- and cysteine-insertion N_6/C_6 half molecules

Results are shown for levels of [^{3}H]MTX uptake in R5 cells and in R5 transfectants expressing *cl*-N_6/C_6 and double cysteine mutants. [^{3}H]MTX (0.5 μM) uptakes were measured for 2 min at 37 °C.

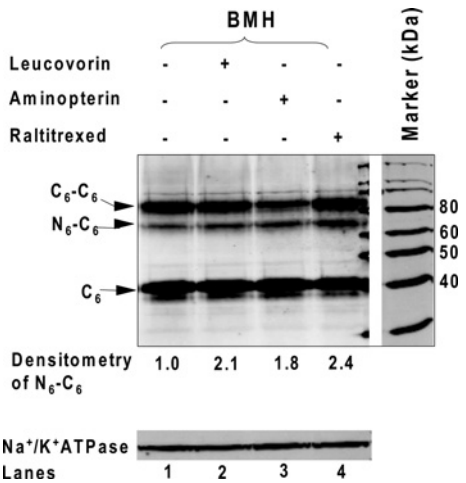

Figure S3 Effects of ligand binding on TMD5/TMD8 cross-linking

Plasma membrane preparations of transfectant of Cys^{175}/Cys^{311} hRFC half-molecules were pretreated with or without 1 mM aminopterin, leucovorin or raltitrexed at 25 °C for 1 h, followed by chemical cross-linking with BMH at 25 °C for 30 min. The immunoblots were probed with anti-Myc antibody and IRDye800-conjugated secondary antibody. Detection and densitometry were performed as described in the Materials and methods section of the main text. C_6 and cross-linked products (C_6–C_6 and N_6–C_6) are noted with arrows. In the lower panel, the blot was stripped and reprobed with an antibody against Na^+/K^+-ATPase as a loading control (mouse antibody from Novus Biologicals). Mean values of N_6–C_6 (normalized to loading control) from four independent experiments are shown below each lane of the image. Relative S.E.M. values were 0.24, 0.18 and 0.30 respectively for the leucovorin, aminopterin and raltitrexed treatments and *P* values compared with the no treatment were all less than 0.02, as measured using a paired *t* test. The molecular mass in kDa is indicated on the right-hand side.

[1] To whom correspondence should be addressed (email matherly@kci.wayne.edu).

Table S1 Primer pairs used for construction of *cI*-N_6, C_6 hRFC, cysteine-substituted mutants and Ser^{313} mutants

Primers	Forward/reverse	Sequences (5′ → 3′)
C30S/C33S	Forward	CGGCGCCTCGTGAGCTACCTTAGCTTCTACGGCTTC
C30S/C33S	Reverse	GAAGCCGTAGAAGCTAAGGTAGCTCACGAGGCGCCG
C220S	Forward	CGACCGGGGGCGGAGCGAAACCTCGGCTTC
C220S	Reverse	GAAGCCGAGGTTTCGCTCCGCCCCCGGTCG
C246S	Forward	CCCTGCGGGTGGCCAGTGGGGACTCAGTGC
C246S	Reverse	GCACTGAGTCCCCACTGGCCACCCGCAGGG
V160C	Forward	TCGCGCGCTGCGTGTCTGCTGGGCGTG
V160C	Reverse	CACGCCCAGCAGACACGCAGCGCGCGA
L161C	Forward	CGCGCTGCGGTGTGTCTGGGCGTGTTC
L161C	Reverse	GAACACGCCCAGACACACCGCAGCGCG
G163C	Forward	GCGGTGCTGCTGTGCGTGTTCACC
G163C	Reverse	GGTGAACACGCACAGCAGCACCGC
V164C	Forward	GTGCTGCTGGGCTGCTTCACCAGCTCC
V164C	Reverse	GGAGCTGGTGAAGCAGCCCAGCAGCAC
S167C	Forward	GGCGTGTTCACCTGCTCCGTGCTG
S167C	Reverse	CAGCACGGAGCAGGTGAACACGCC
S168C	Forward	GTGTTCACCAGCTGCGTGCTGGGC
S168C	Reverse	GCCCAGCACGCAGCTGGTGAACAC
G171C	Forward	AGCTCCGTGCTGTGCCAGCTGCTG
G171C	Reverse	CAGCAGCTGGCCGCACACGGAGCTGGT
Q172C	Forward	TCCGTGCTGGGCTGTCTGCTGGTCACT
Q172C	Reverse	AGTGACCAGCAGACAGCCCAGCACGGA
L174C	Forward	CTGGGCCAGCTGTGTGTCACTGTGGGC
L174C	Reverse	GCCCACAGTGACACACAGCTGGCCCAG
V175C	Forward	GGCCAGCTGCTGTGCACTGTGGGCCGA
V175C	Reverse	TCGGCCCACAGTGCACAGCAGCTGGCC
A311C	Forward	GCGGCAGATTGTGCCTCCACGCTGC
A311C	Reverse	GCAGCGTGGAGGCACAATCTGCCGC
T314C	Forward	GATGCTGCCTCCTGTCTGCTGGGCG
T314C	Reverse	CGCCCAGCAGACAGGAGGCAGCATC
L315C	Forward	GCCTCCACGTGCCTGGGCGCCATCAC
L315C	Reverse	GTGATGGCGCCCAGGCACGTGGAGGC
G317C	Forward	TCCACGCTGCTGTGTGCCATCACGTCC
G317C	Reverse	GGACGTGATGGCACACAGCAGCGTGGA
A318C	Forward	CTGCTGGGCTGCATCACGTCCTTCGC
A318C	Reverse	GCGAAGGACGTGATGCAGCCCAGCAG
S321C	Forward	GCCATCACGTGCTTCGCCGCGGGCTTCG
S321C	Reverse	CGAAGCCCGCGGCGAAGCACGTGATGGC
F322C	Forward	GCCATCACGTCCTGCGCCGCGGGCTTCG
F322C	Reverse	CGAAGCCCGCGGCGCAGGACGTGATGGC
G325C	Forward	TCCTTCGCCGCGTGCTTCGTGAAGATCCGC
G325C	Reverse	GCGGATCTTCACGAAGCACGCGGCGAAGGA
F326C	Forward	TTCGCCGCGGGGCTGTGTGAAGATCC
F326C	Reverse	GGATCTTCACACAGCCCGCGGCGAA

Received 1 February 2010/8 June 2010; accepted 17 June 2010
Published as BJ Immediate Publication 17 June 2010, doi:10.1042/BJ20100181